Proceedings of the ASME 2016 International Design Engineering Technical Conferences & Computers and Information in Engineering Conference
IDETC/CIE 2016
August 21-24, 2016, Charlotte, North Carolina

IDETC2016-59388

DESIGN AND ANALYSIS OF A ROBOTIC MODULAR LEG MECHANISM

Wael Saab
Robotics and Mechatronics Laboratory
Virginia Tech
Blacksburg, VA 24061

Pinhas Ben-Tzvi
Robotics and Mechatronics Laboratory
Virginia Tech
Blacksburg, VA 24061
bentzvi@vt.edu

ABSTRACT

This paper presents the design and analysis of a reduced degree-of-freedom Robotic Modular Leg (RML) mechanism used to construct a quadruped robot. This mechanism enables the robot to perform forward and steering locomotion with fewer actuators than conventional quadruped robots. The RML is composed of a double four-bar mechanism that maintains foot orientation parallel to the base and decouples actuation for simplified control, reduced weight and lower cost of the overall robotic system. A passive suspension system in the foot enables a stable four-point contact support polygon on uneven terrain. Foot trajectories are generated and synchronized using a trot and modified creeping gait to maintain a constant robot body height, horizontal body orientation, and provide the ability to move forward and steer. The locomotion principle and performance of the mechanism are analyzed using multi-body dynamic simulations of a virtual quadruped and experimental results of an integrated RML prototype.

1 INTRODUCTION

In recent years, there has been a surge of research conducted in the field of multi-legged robotics due to the high adaptability of legged locomotion on unstructured terrain [1-4]. Conventional multi-legged robotic designs consist of a large number of active degrees of freedom (DOF) that enhance locomotion and tasking abilities; however, this increases the robots weight, energy consumption and increases the difficulty of trajectory planning and control [5, 6]. Therefore, if leg mechanisms can be designed with reduced-DOF yet achieve the same walking abilities, they can be constructed in lighter weight, reduced cost and improved controllability making them of more practical use.

The majority of multi-legged robots are bio-inspired from animals that have evolved over the years to adapt to their natural habitats. These robots utilize multi-DOF leg mechanisms to arbitrarily position their single point of contact feet to perform forward walking gaits and steer on both flat and uneven terrain. Therefore, a $2n$-legged robot requires $6n$ actuators where n is the number of leg pairs [7]. If flat feet are to be implemented into leg mechanism to enhance stability and disturbance rejection capabilities [8], additional DOFs are required to control foot orientation during a walking gait.

To address these issues, researchers have investigated methods to reduce the number of actuated leg joints in multi-legged robotic systems. Torige et al. developed a six-segment centipede type walking robot with four motors required per segment. In this design, point contact was sufficient to provide a stable support polygon since a minimum of three feet were in contact with the ground during a walking gait. Therefore, a $2n$ legged robot utilized $4n$ active joints [9]. Similarly, Hoffman et al. designed a micro scale centipede robot with passive revolute joints located between repeated two-legged segments. The legs of each segment were coupled to two linear actuators that provide opposing moments about the center of mass (COM) causing the body to extend, raise the legs and the robot forward [10]. The Rhex hexapod robot was designed with six actuated DOF that continuously rotate compliant C-shaped legs that propel the robot forward [11]. A similar design concept was implemented on centipede robot with an active DOF between its body segments each utilizing a continuously rotating link acting as a leg [12]. Yoenda et al. designed a quadruped robot with four active DOF. The quadruped body was separated into a front and rear section connected using an active revolute joint that can roll in the horizontal direction. Roll motion of the body coupled with rotation of U-shaped front and rear legs with point contact feet caused the robot to move forward [13]. However, robot could only perform a creep gait.

This paper investigates the performance of a reduced DOF Robotic Modular Leg (RML) mechanism. The RML is composed of a double four bar mechanism that provides benefits of simplified control through actuation decoupling and maintains a constant flat foot orientation throughout its entire trajectory without the use of an additional actuator. A passive suspension system ensures a stable four-point contact support polygon and walking on uneven terrain. Gait patterns for a quadruped robot are developed to provide the robot forward locomotion and steering capabilities. The aim of this research is to develop a reduced DOF multi-legged platforms that can be used to investigate performance improvements that robotic tails can bring about these robotic systems [14-19] in terms of stability and maneuverability.

This paper is organized as follows. Section 2 presents the mechanical design concept of the RML and the quadruped configuration. Section 3 presents kinematic analysis of the proposed mechanism. Section 4 presents a list of walking ability performance criteria in terms of body stability, forward and turning locomotion capabilities used to generate foot trajectories to produce a stable walking gait. Section 5 presents gait walking patterns to achieve forward and steering locomotion. Section 6 presents dynamic simulations used to evaluate the performance of the proposed mechanism and select mechanical components for proper operation. Section 7 presents experimental results of an integrated prototype. Concluding remarks and future work are discussed in Section 8.

2 MECHANICAL DESIGN

This section presents the mechanical design of the RML and how it is configured to build a quadruped robot. Figure 1 shows a side view schematic diagram of the RML. The mechanism is composed of double four bar mechanisms with two DOFs that constitute the thigh and shin. The thigh rotates about the hip joint and the shin rotates about the knee joints. The four bar mechanisms have two equal short and long linkages resulting in a double rocker configuration. Therefore, the orientation of the body is propagated throughout the mechanism and maintains a constant parallel orientation of a flat foot. This results in a flat foot orientation that is controlled without the use of an actuator. Flat feet provide a more stable support polygon in comparison to point or line contact feet [20].

One of the main benefits of using four bar is the advantage of actuation decoupling. The thigh is actuated directly by a motor mounted within the body while shin is actuated by a motor mounted within a linkage of the thigh and transfers its torque to the shin using a 1:1 timing belt system. This motor configuration enables a relative input to the shin with respect to the thigh; further simplifying control without the need of input compensation due to its decoupled nature. In addition, this enables the motors to be placed within or near the vicinity of the body; minimizing leg inertia for improved response time. This also aids the assumption of concentrated body mass and massless legs for modeling of the mechanisms equations of motion.

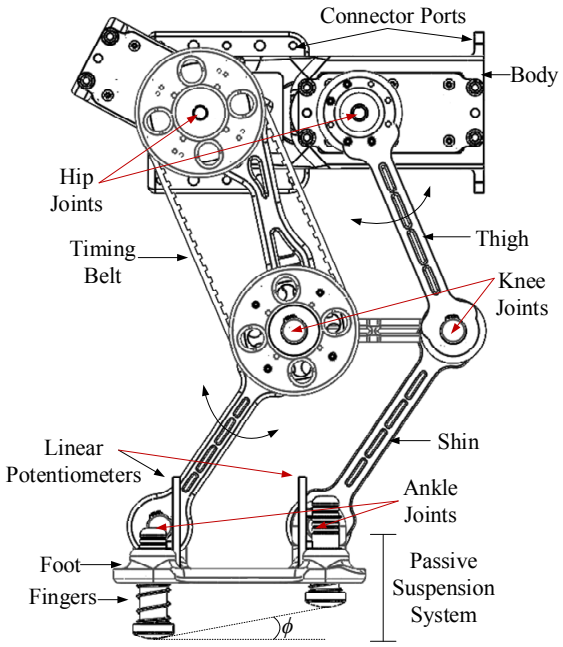

Figure 1. Side view schematic diagram of the RML

A passive suspension system, inspired by the active locking foot mechanism in [21], is integrated into the foot that permits vertical translation of four fingers. Compression springs installed between each finger and the foot provide compliance that softens impact and maintains a stable support polygon with four points of contact, even in the presence of uneven terrain. Shock absorbent gel pads are placed at the end of each finger to further increase compliance, contact surface area and contact friction to reduce slipping. A linear pattern of retaining ring groves is incorporated into the fingers to adjust the springs pre-compression. Linear potentiometers measure spring deflection of each finger. This sensory feedback information can be used to determine the contact forces with the ground and to calculate the zero moment point stability criteria of the legged robot [22]. The passive suspension system enables the RML to walk on uneven terrain with a maximum inclination angle ϕ when two fingers in the same plane are in fully extended and compressed states as depicted in Fig. 1. ϕ is dependent on foot geometry and the stroke length of each spring after pre-compression.

Design symmetry of the structural components of the RML enable the construction of multi-legged robots by interconnecting identical modules via its connector ports, Fig. 1. Figure 2 shows an isometric view of a quadruped configuration that is constructed from four RMLs. Extension units have been used to modify the overall length of the robotic system. A biped configuration can also be constructed by connecting two RMLs; however, the legged robot will require an addition DOF (i.e. robotic tail [14-19], swaying torso [23], fly wheel [24]…) to perform a stable walking gait and maneuver. A biped configuration may also be formed by interconnected two RML mechanisms.

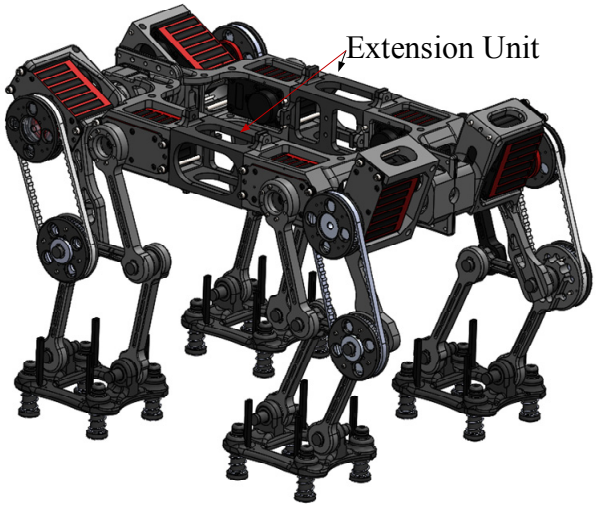

Figure 2. Isometric view of a Quadruped configuration

3 KINEMATIC ANALYSIS

Forward kinematics utilizes prescribed angles in the joint-space to compute the task-space pose of the foot with respect to a coordinate frame X_0Y_0 attached to the body as seen in Fig. 3. Let X_1Y_1 be a coordinate from attached to the foot. Therefore, forward kinematics of the RML can be represented using the homogeneous transformation matrix [25].

$$A_1^0 = \begin{pmatrix} I & \begin{matrix} l_1\cos\theta_1 + l_2\cos(\theta_1+\theta_2) \\ l_1\sin\theta_1 + l_2\sin(\theta_1+\theta_2) \end{matrix} \\ 0 \quad\quad 1 \end{pmatrix} \tag{1}$$

Where l_1, l_2 and θ_1, θ_2 represent the lengths and relative angle of the thigh and shin respectively.

Inverse kinematics calculates the joint-space angles from a prescribed task-space foot pose. Inverse kinematics is a more challenging problem to solve since forward kinematic equations may be nonlinear where multiple joint configurations may constitute a single known pose. This means a solution may neither be unique or easy to compute. In general inverse kinematics may be solved geometrically (solving for angles directly from the mechanism geometry), analytically (manipulating the forward kinematics to solve for the joint angles) or iteratively (using numerical analysis). In this paper, a geometric approach is used to solve the inverse kinematics problem [25].

Given a known foot position, P_x and P_y, with respect to X_0Y_0 there exist two solutions representing knee-forward and knee-reverse configurations if l_1 and l_2 are not parallel. If l_1 and l_2 are parallel, there exist infinite solutions if X_0Y_0 and X_1Y_1 coincide; otherwise, there is one solution. Figure 2 depicts RML in the knee-forward configuration. The inverse kinematic equations for the RML are derived geometrically using the law of cosines and trigonometry identities shown in the equations below:

$$C = \cos\theta_2 = \frac{P_x^2 + P_y^2 - l_1^2 - l_2^2}{2l_1l_2}$$

$$\theta_2 = \tan^{-1}\frac{\sin\theta_2}{\cos\theta_2} = \pm\tan^{-1}\frac{\sqrt{1-C^2}}{C} \tag{2}$$

$$\theta_1 = a\tan 2(P_y, P_x) - \tan^{-1}\left(\frac{l_2\sin\theta_2}{l_1 + l_2\cos\theta_2}\right)$$

We notice that θ_1 is dependent on θ_2, this physically makes sense since the value of θ_1 depends on which solution (knee-forward or knee-reverse) is chosen for θ_2.

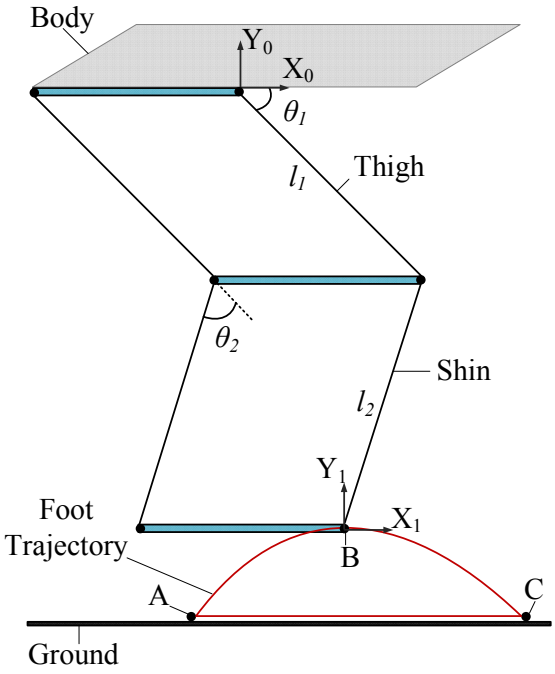

Figure 3. Simplified schematic diagram of a RML following a foot trajectory.

4 TRAJECTORY PLANNING

This section presents trajectory planning of the RML leg to maintain a stable, constant body height and forward velocity with respect to the ground with minimal ground impact loading. Trajectory planning involves the process of generating foot trajectories in space relative to the fixed body coordinate frame.

Figure 3 shows a complete single-cycle foot trajectory that consists of two main phases: swing and support phase represented by segments A-B-C and C-A respectively. The swing phase advances the foot forward while the support phase supports the robot at the ground and propels the robot body forward. Point A and C are takeoff and landing points for the foot.

In this paper, the following minimum set of walking ability criteria [26] is used as achievable performance criteria to assess

performance of the quadruped configuration and generate desirable foot trajectories to produce locomotion. These criteria are listed as follows: (i) maintain quasi-static equilibrium, (ii) maintain a constant robot body height during a walking gait, (iii) maintain a horizontal body orientation during a walking gait, (iv) move forward and steer. Criteria (i) and (ii) are required to maintain a stable robotic platform in static configurations and during a walking gait and improve energy efficiency. Criterion (iii) ensures a sufficient COM margin of stability within the support polygon defined as the convex hull of the robot's feet in contact with the ground. Criterion (iv) ensures the robot can be steered in any desired position and direction. Criteria (i) and (iv) will be addressed in Section 5.

In order to achieve criteria (ii) and (iii) for flat-terrain walking, it is required to have a straight line support phase, with respect to the body coordinate frame that is free of vertical translation of the passive suspension system fingers and impulsive forces at takeoff and landing instances. Vertical translation of the fingers will cause changes in body height and impulsive forces transmitted to the body will cause the body to deviate from its horizontal configuration. To prevent vertical finger translation, spring pre-compressions will be adjusted such that the summation of spring forces equal the weight of a single RML mechanism. Therefore, the robot body height will remain constant while walking since the suspension system will only dissipate energy in the presence of impulsive loading. To minimize impulsive forces, foot trajectories require zero vertical velocity and acceleration at takeoff and landing instances while the robot height is held constant. Therefore, quintic polynomials shown in Eq. 3 are used to specify foot trajectory position, velocity and acceleration $\{q(t), v(t), \alpha(t)\}$

$$\begin{aligned} q(t) &= a_0 + a_1 t + a_2 t^2 + a_3 t^3 + a_4 t^4 + a_5 t^5 \\ v(t) &= a_1 + 2a_2 t + 3a_3 t^2 + 4a_4 t^3 + 5a_5 t^4 \\ \alpha(t) &= 2a_2 + 6a_3 t^1 + 12a_4 t^2 + 20a_5 t^3 \end{aligned} \tag{3}$$

By setting initial and final conditions, Eq. 3 can be expressed in matrix notation as a linear set of 6 equations and 6 scalar unknowns (a_i),

$$\begin{bmatrix} 1 & t_0 & t_0^2 & t_0^3 & t_0^4 & t_0^5 \\ 0 & 1 & 2t_0 & 3t_0^2 & 4t_0^3 & 5t_0^4 \\ 0 & 0 & 2 & 6t_0 & 12t_0^2 & 20t_0^3 \\ 1 & t_f & t_f^2 & t_f^3 & t_f^4 & t_f^5 \\ 0 & 1 & 2t_f & 3t_f^2 & 4t_f^3 & 5t_f^4 \\ 0 & 0 & 2 & 6t_f & 12t_f^2 & 20t_f^3 \end{bmatrix} \begin{bmatrix} a_0 \\ a_1 \\ a_2 \\ a_3 \\ a_4 \\ a_5 \end{bmatrix} = \begin{bmatrix} q_0 \\ v_0 \\ \alpha_0 \\ q_f \\ v_f \\ \alpha_f \end{bmatrix} \tag{4}$$

Eq. 4 can be solved to generate foot trajectories for the swing phase divided into two segments: A-B and B-C. Initial and final conditions $\{q_0, v_0, \alpha_0\}$ and $\{q_f, v_f, \alpha_f\}$, at t_0 and t_f respectfully, were set to complete the swing phase in 1.5 seconds with a step height of 5 cm and a step length = 15 cm. The resulting horizontal foot velocity is equivalent to 0.1 m/s. Trajectory plots were computed using these parameters. Figure 4 shows trajectory plots of vertical foot position, velocity and acceleration versus time for a single swing cycle. Smooth trajectories are observed over the entire step cycle with zero velocities and accelerations at the takeoff and landing instances; thus ensuring minimal impulsive impact forces between the ground and foot. A linear equation was used to generate the trajectory for the support phase. A vector of horizontal position points computed to provide constant horizontal velocity was concatenated with the vertical foot trajectory position points to move the body forward and complete the entire foot trajectory cycle. Joint trajectory profiles were then computed using inverse kinematic relations in Eq. 2.

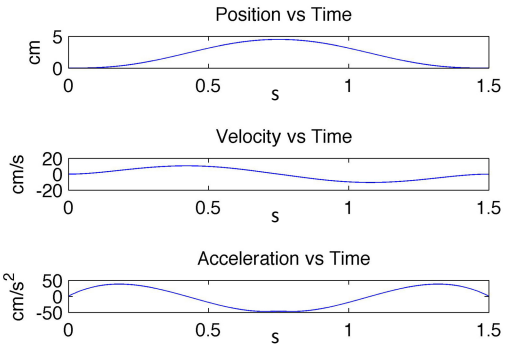

Figure 4. Computed trajectory plots of vertical foot position, velocity, and acceleration versus time for a single swing cycle

5 LOCOMOTION PRINCIPLE

In this section two gait patterns are presented to sequence leg motions and provide the quadruped with statically stable walking gaits and the ability to move forward and steer. These walking abilities represent criteria (i) and (iv) defined in Section 4.

The quadruped must perform its foot trajectories within a specific sequence (i.e. gait pattern) to provide stable forward and steering capabilities. It has been shown that for a quadruped with flat feet trot and creeping gait patterns can provide a statically stable walking gaits [27]. The trot gait pattern will be used to provide forward locomotion and a modified creeping gait will be used to provide differential steering [28] of the robot where only one leg performs *n*-cycles of its desired foot trajectory while the remaining legs are held stationary.

Figure 5 shows the gait diagram of the quadruped configuration for the trot walking gait. The horizontal axis of the plot indicates the normalized time T of a complete foot trajectory cycle. The bold line segment associated with each leg starts from landing and ends at takeoff instances. These line segments indicate the period of the support phase. From this diagram, we can define gait parameters of leg i: duty cycle ϕ_i and phase ψ_i.

$$\phi_i = \frac{\text{Support period of leg } i}{T}$$
$$\psi_i = \frac{\text{Landing time of leg } i}{T} \quad (5)$$

For the quadruped configuration trot gait pattern, landing time of leg i is measured from the instant of landing of leg 1; therefore $\{\psi_1 = 0\}$ and $\{\phi_{1\text{-}4} = \psi_2 = \psi_3 = 0.5, \psi_4 = 0\}$.

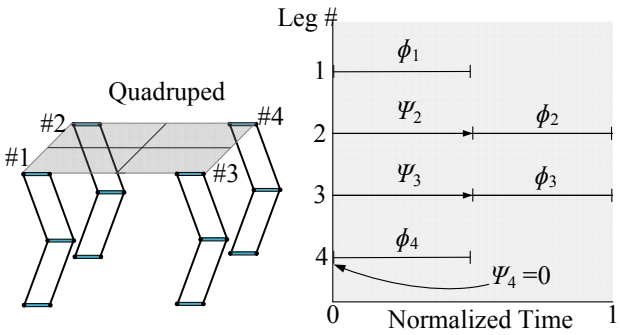

Figure 5. Trot gait diagram of the quadruped configuration.

For the modified creep gait, a case study is presented to demonstrate how steering is achieved. Figure 6 shows a simplified model of the quadruped robot. The robot is oriented at a heading angle, α, and is capable of translating in the xy plane. Let leg 3 perform a foot trajectory that produces an input friction force F_v that is equivalent to $\mu F_N \text{sgn}(v)$. Where μ is the coefficient of friction, v is the horizontal foot velocity and F_N is the normal contact force equivalent to the summation of spring forces in the foot. F_v is directed along the length of the robot and opposes foot velocity, v, during the support phase force. It is assumed that the weight of the robot is evenly distributed about its feet and that F_v is located at the corner of the robot. Using the generalized coordinates $\{x, y, \alpha\}$, the equations of motion of the system are derived using the Lagrangian formulation, with friction modeled as non-conservative forces [29], given by

$$M\ddot{x} + b_1\dot{x} = F_v \cos\alpha$$
$$M\ddot{y} + b_2\dot{y} = F_v \sin\alpha \quad (6)$$
$$I\ddot{\alpha} + b_3\alpha = F_v w/2$$

Where M and I are the mass and moment of inertia of the quadruped, b_i are damping coefficients, and w is the width of the quadruped. Solving Eq. 6 yields an estimated value of heading angle and position trajectory of the quadruped since friction is being modeled as a force linearly proportional to velocity. This simplifying assumption avoids nondeterministic dynamics if a more accurate friction model is adopted [30].

Simulation model parameters M = 18.8 kg, I = 1 kg·m^2, w = 0.35 m were obtained from a CAD model of the quadruped. Friction parameters were estimated based on material properties as μ = 0.1 and b_i = 1 N-s/m. The accuracy of these estimates can be improved with experimental results [31]. Using these parameters, Eq. 6 was solved for a single foot trajectory cycle with a support phase duration of 1.5 s. Results indicated a heading angle change equivalent to $\Delta\alpha$ = 6.5° with COM translation equivalent to Δx = 6.7 cm, and Δy = 0.1 cm.

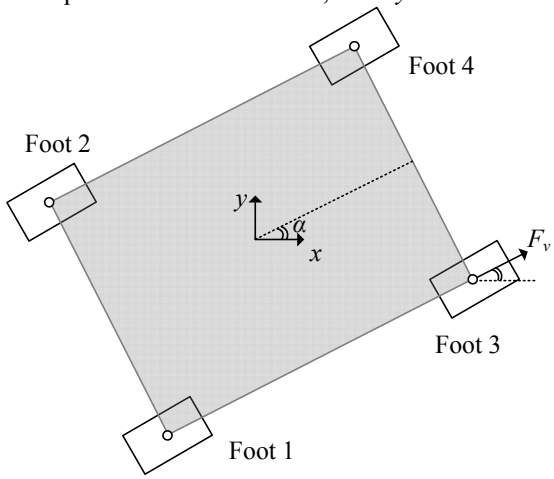

Figure 6. Simplified model of the quadruped configuration.

6 DYNAMIC SIMULATIONS

In this section, dynamic simulations are analyzed to evaluate the performance of the RML. When designing robotic systems, it is required to understand how various components interact and determine forces/moments generated during operation to prevent mechanical failure of an integrated prototype. Dynamic simulations provide a tool to test and analyze virtual robotic systems before building a physical prototype; thus, dramatically reducing development cost and time. A 3D assembly of the quadruped configuration was built using CAD software and exported to MSC ADAMS, a physics-based multi-body dynamic motion simulation software. The simulations accounted for inertia, mass distributions of the robot (i.e. linkages, motors, and electronics), spring pre-compression, link accelerations, body contact, and frictional forces between the feet and ground.

Data pertaining to dynamic motion simulations was analyzed for the following purposes: (1) to analyze the robot's trot and modified creeping walking gait to perform planar walking and steering using foot trajectories generated in Section 4, and (2) to analyze the required joint torque and angular velocities for motor selection.

6.1 Simulation Results and Analysis

Figure 7 shows a side view of the quadruped configuration performing the trot gait pattern (described in Section 5) on both smooth and uneven terrain. Uneven terrain consisted of triangular peaks of 8 cm height and rounded surfaces of fillet

size equal to 1 cm. The quadruped successfully walks with a constant forward velocity equivalent to 0.1 m/s on smooth terrain while maintaining a horizontal body orientation and height with respect to the floor. However, on uneven terrain, slight swaying in the roll and pitch directions and fluctuations in body height was observed due to spring deflection in the feet resulting from variations in ground height; in addition, slipping occurred at some instances that slightly reduced the forward walking velocity. These undesirable effects are expected to increase with the amount of unevenness of the terrain. The suspension system successfully maintained a stable four point of contact support polygon at each foot and provided static stability on both terrains.

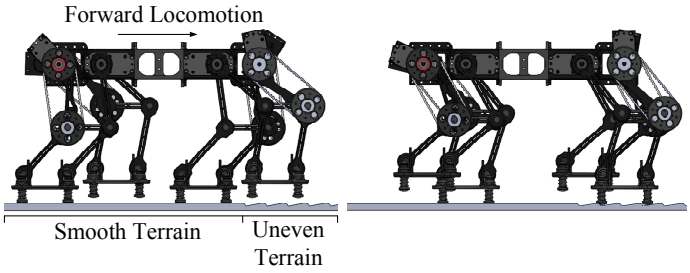

Figure 7. Adams model simulation of quadruped robot performing the trot gait pattern on both smooth and uneven terrain.

Figure 8 shows a top view of the quadruped configuration performing the modified creeping gait where Leg 3 performs a single foot trajectory cycles to steer the robot while the reaming legs are held stationary. The cycle caused rotation and translation of the robot body equivalent to $\Delta\alpha = 4.25°$, $\Delta x = 4$ cm, and $\Delta y = 2$ cm. Simulation results fall slightly below computed values from Section 6 due to simplifying assumptions.

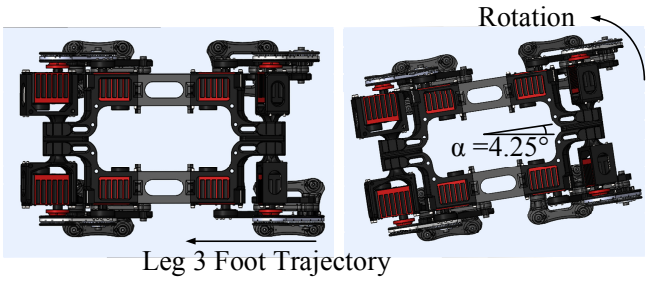

Figure 8. Top view of the quadruped configuration performing the modified creeping gait to steer the robot.

In order to select the proper motor, joint torques and angular velocities were measured during trot walking gait on smooth terrain. Figure 9 shows angular velocity and torque requirements of a RML located at the left, backside of the quadruped. From these plots, the maximum torque and angular velocity is identified that represents maximum values motors must provide to achieve the given walking gait. A safety factor, n=2, was used for evaluating the maximum peak torque that may represent highest torque requirements for payload carrying capabilities, or unexpected external loading. Based on the maximum measured angular velocity and peak torque, servomotors were selected for both the hip and knee joints that can provide 11.3 N-m and 120 deg/s.

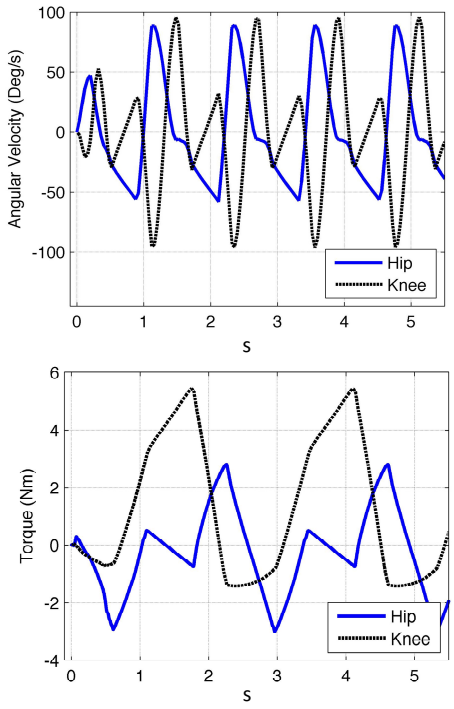

Figure 9. Angular velocity and torque requirements of a RML located at the left, backside of the quadruped.

7 EXPERIMENTAL RESULTS

In this section, experiments are carried out on an integrated prototype shown in Fig. 10 to evaluate the performance of the RML in performing walking gaits. Structural components were fabricated using 3D printing with ABS thermoplastic. Servo motors were selected based on simulation results of Section 7. The prototype's weight is 4.7 kg. Springs of stiffness K = 4.6 N/mm and stroke length of 25 mm were used for the passive suspension system. Spring pre-compression was adjusted to 2.5 mm to equate the spring forces with the weight of the RML mechanism to maintain a constant body height when used to construct the quadruped configuration during the support phase. The foot is capable of maintaining a four-point of contact support polygon in the presence of uneven terrain with a maximum inclination angle measured to be ϕ = 14.5º.

A Teensy 3.1 MCU was connected to a computer via a USB-serial port and used to send joint trajectories to the RML servomotors. To ensure stable response of servo motors, the joint trajectories profiles were sampled at an update rate of 50 Hz using linear interpolation.

The RML prototype successfully tracked a foot trajectory with a step height = 5 cm, step length = 15 cm at a foot horizontal velocity equivalent to 0.1 m/s as seen in Fig. 10. However, backlash in the timing belt caused the RML foot to deviate approximately 2 cm from the straight line support phase of the gait trajectory.

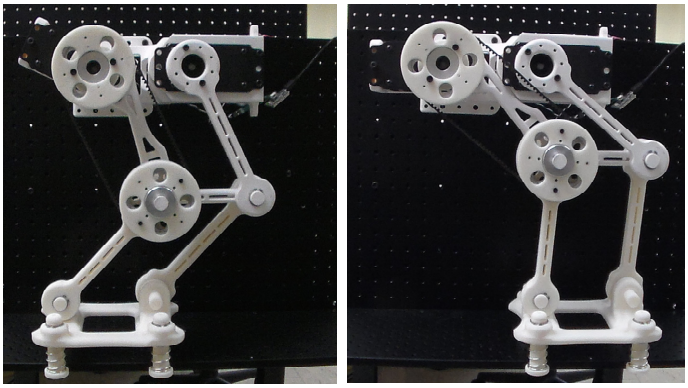

Figure 10. Integrated prototype of the RML performing a walking gait.

8 CONCLUSION

The work presented here investigates the performance of a reduced DOF RML mechanism used to construct a quadruped robotic structure. The RML is composed of double four bar mechanisms that provides the advantages of actuation decoupling and maintains parallel foot orientation for simplified control, reduced weight and lower cost. A passive suspension system maintains a stable four-point of contact support polygon and the ability to traverse uneven terrain. Walking ability performance criteria was used to evaluate the mechanism and generate foot trajectories to provide static stability, maintain a constant robot body height, maintain a horizontal body orientation, provide the ability to more forward and steer. Dynamic simulations were developed to evaluate performance of a virtual quadruped prototype. Results indicate that the RML is capable of satisfying all performance criteria on smooth terrain; however, pitch and roll swaying of the body and fluctuations in body height were observed due to variations in ground height. Experimental results indicated that the RML can track the generated foot trajectory with slight deviations observed during the support phase due to the timing belt backlash.

Future work will involve developing both biped and quadruped prototypes using the RML to provide a stable experimental platform to investigate the performance advantages a robotic tail can provide these legged robots. Methods to eliminate backlash of the timing belt system will further be investigated to accurately track foot trajectories and provide an idealized straight line support phase. Multi-body dynamic simulations will be used to develop hardware in the loop experiments to further evaluate the performance improvements of robotic tails attached to multi-legged robots.

ACKNOWLEDGMENTS

This material is based upon work supported by the National Science Foundation under Grant No. 1557312.

REFERENCES

[1] Silva, M. F., and Machado, J. T., 2007, "A Historical Perspective of Legged Robots," Journal of Vibration and Control, 13(9-10), pp. 1447-1486.

[2] Song, S.-M., and Waldron, K. J., 1989, Machines That Walk: The Adaptive Suspension Vehicle, MIT press.

[3] Arikawa, K., and Hirose, S., 2007, "Mechanical Design of Walking Machines," Philosophical Transactions of the Royal Society of London A: Mathematical, Physical and Engineering Sciences, 365(1850), pp. 171-183.

[4] Machado, J. T., and Silva, M. F., 2006, "An Overview of Legged Robots," *Proc. International Symposium on Mathematical Methods in Engineering*.

[5] Galvez, J. A., Estremera, J., and De Santos, P. G., 2003, "A New Legged-Robot Configuration for Research in Force Distribution," Mechatronics, 13(8), pp. 907-932.

[6] Chen, X., Wang, L.-q., Ye, X.-f., Wang, G., and Wang, H.-l., 2013, "Prototype Development and Gait Planning of Biologically Inspired Multi-Legged Crablike Robot," Mechatronics, 23(4), pp. 429-444.

[7] Tang, Y., Ma, S., Sun, Y., and Ge, D., 2012, "A Multi-Legged Robot with Less Actuators by Applying Passive Body Segment Joint," *Proc. Intelligent Robots and Systems*, IEEE, pp. 1828-2833.

[8] Schwab, A., and Wisse, M., 2001, "Basin of Attraction of the Simplest Walking Model," *Proc. ASME 2001 International Design Engineering Technical Conferences and Computers and Information in Engineering Conference*, ASME, pp. 531-539.

[9] Torige, A., Noguchi, M., and Ishizawa, N., 1993, "Centipede Type Multi-Legged Walking Robot," *Proc. Intelligent Robots and Systems*, IEEE, pp. 567-571.

[10] Hoffman, K. L., and Wood, R. J., 2011, "Passive Undulatory Gaits Enhance Walking in a Myriapod Millirobot," *Proc. IEEE/RSJ International Conference on Intelligent Robots and Systems* IEEE, pp. 1479-1486.

[11] Saranli, U., Buehler, M., and Koditschek, D. E., 2001, "Rhex: A Simple and Highly Mobile Hexapod Robot," The International Journal of Robotics Research, 20(7), pp. 616-631.

[12] Jimenez, B., and Ikspeert, A., 2007, "Centipede Robot Locomotion," Master's thesis, Ecole Polytechnique Federale de Lausanne.

[13] Yoneda, K., OTA, Y., Ito, F., and Hirose, S., 2000, "Construction of a Quadruped with Reduced Degrees of Freedom," *Proc. Industrial Electronics Society*, IEEE, pp. 28-33.

[14] Rone, W. S., and Ben-Tzvi, P., 2014, "Continuum Robot Dynamics Utilizing the Principle of Virtual Power," Transactions on Robotics, 30(1), pp. 275-287.

[15] Rone, W. S., and Ben-Tzvi, P., 2014, "Mechanics Modeling of Multisegment Rod-Driven Continuum

Robots," Journal of Mechanisms and Robotics, 6(4), p. 041006.
[16] Rone, W. S., and Ben-Tzvi, P., 2014, "Continuum Robotic Tail Loading Analysis for Mobile Robot Stabilization and Maneuvering," *Proc. International Design Engineering Technical Conferences and Computers and Information in Engineering Conference*, ASME, pp. V05AT08A009-V005AT008A009.
[17] Rone, W. S., and Ben-Tzvi, P., 2013, "Multi-Segment Continuum Robot Shape Estimation Using Passive Cable Displacement," *Proc. IEEE International Symposium on Robotic and Sensors Environments* IEEE, pp. 37-42.
[18] Rone, W. S., and Ben-Tzvi, P., 2012, "Continuum Manipulator Statics Based on the Principle of Virtual Work," *Proc. International Mechanical Engineering Congress and Exposition*, ASME pp. 321-328.
[19] Rone, W. S., and Ben-Tzvi, P., 2015, "Static Modeling of a Multi-Segment Serpentine Robotic Tail " *Proc. ASME 2015 International Design Engineering Technical Conferences and Computers and Information in Engineering Conference*, ASME.
[20] Schwab, A., and Wisse, M., "Basin of Attraction of the Simplest Walking Model," *Proc. Proceedings of the ASME Design Engineering Technical Conference*, pp. 531-539.
[21] Hashimoto, K., Hosobata, T., Sugahara, Y., Mikuriya, Y., Sunazuka, H., Kawase, M., Lim, H.-o., and Takanishi, A., 2005, "Development of Foot System of Biped Walking Robot Capable of Maintaining Four-Point Contact," *Proc. IEEE/RSJ International Conference on Intelligent Robots and Systems*, IEEE, pp. 1361-1366.
[22] Vukobratović, M., and Borovac, B., 2004, "Zero-Moment Point—Thirty Five Years of Its Life," International Journal of Humanoid Robotics, 1(01), pp. 157-173.
[23] Haruna, M., Ogino, M., Hosoda, K., and Asada, M., 2001, "Yet Another Humanoid Walking-Passive Dynamic Walking with Torso under Simple Control," *Proc. IEEE/RSJ International Conference on Intelligent Robots and Systems*, IEEE, pp. 259-264.
[24] Wong, T. C., and Hung, Y. S., 1996, "Stabilization of Biped Dynamic Walking Using Gyroscopic Couple," *Proc. IEEE International Joint Symposia on Intelligence and Systems*, IEEE, pp. 102-108.
[25] Spong, M. W., Hutchinson, S., and Vidyasagar, M., 2006, Robot Modeling and Control, Wiley New York.
[26] Kaneko, M., Abe, M., Tachi, S., Nishizawa, S., Tanie, K., and Komoriya, K., 1985, "Legged Locomotion Machine Based on the Consideration of Degrees of Freedom," Theory and Practice of Robots and Manipulators, Springer, pp. 403-410.
[27] Kajita, S., and Espiau, B., 2008, "Legged Robots," Springer Handbook of Robotics, Springer, pp. 361-389.
[28] Pullin, A. O., Kohut, N. J., Zarrouk, D., and Fearing, R. S., 2012, "Dynamic Turning of 13 Cm Robot Comparing Tail and Differential Drive," *Proc. IEEE International Conference on Robotics and Automation* IEEE, pp. 5086-5093.
[29] Riewe, F., 1996, "Nonconservative Lagrangian and Hamiltonian Mechanics," Physical Review E, 53(2), p. 1890.
[30] Szalai, R., and Jeffrey, M. R., 2014, "Nondeterministic Dynamics of a Mechanical System," Physical Review E, 90(2), p. 022914.
[31] Fritzen, C.-P., 1986, "Identification of Mass, Damping, and Stiffness Matrices of Mechanical Systems," Journal of Vibration and Acoustics, 108(1), pp. 9-16.

